PNAS
www.pnas.org

Supplementary Information for

Routing information flow by separate neural synchrony frequencies allows for 'functionally labeled lines' in higher primate cortex

Mohammad Bagher Khamechian, Vladislav Kozyrev, Stefan Treue*, Moein Esghaei, Mohammad Reza Daliri*

* Mohammad Reza Daliri, Stefan Treue
Email: daliri@iust.ac.ir, treue@gwdg.de

This PDF file includes:

Supplementary text
Figs. S1 to S15
References for SI reference citations

www.pnas.org/cgi/doi/10.1073/pnas.1819827116

Supplementary Information Text

Temporal evolution of SPC. We calculated SPC for the time interval of 1000ms before the stimulus change. Similar to the original analysis, the fast and slow trials which were equal in high-gamma power (195-200 Hz, which was associated to the maximum modulation-see Fig. 1A) and spike rates, were selected (*see Methods*). We used a sliding window with 250ms length, and steps of 125ms to investigate the temporal dynamics of SPC strength. To this end, the SPC was calculated for the time windows of a given trial. Then, we averaged SPC per time window across trials. We repeated the algorithm for 100 times (to consider different spike shuffles) in order to reach a reliable time-resolved SPC. Furthermore, we calculated a spike density function (SDF) by convolving the spike trains with a Gaussian kernel function (50ms standard deviation). SDFs were calculated for each trial and averaged across trials. Fig. S4 shows the time course of SPC and the SDF for the fast and slow trials. As shown in Fig. S4A, the SPC difference between fast and slow trials is observed as early as around a second before the change event. Further, it is visually evident that strength of the SPC is always higher in the fast rather than slow trials. Conversely, the fast and slow trials do not show a significant difference in SDF throughout the analysis interval ($p>0.038$, two-sided rank-sum test with FDR correction, Fig. S4B).

SPC strength is not an artifact of transient activity changes. We provide a visualization and quantification of the raw data to investigate temporal dynamics of spike density function (SDF) and LFP's power for the two behavioral conditions (Fig. S5 & Fig. S6). To this end, we calculated the SDF and time-frequency spectrum for fast and slow trials using LFP signals. The short-time Fourier transform (STFT) with 50 ms time windows overlapped by 45ms was employed to estimate the time-frequency spectrogram. Next, each trial's time-frequency map was normalized by its maximum power. We calculated the average STFT maps (across trials) for the frequency range 150-300 Hz, covering the range with a significant SPC difference between fast and slow trials (see Fig. 1A-C). Furthermore, we calculated the normalized SDF for each unit. To this end, the spike train in each trial was convolved by a Gaussian kernel (10ms standard deviation) and normalized by the maximum value per trial. Next, SDFs were averaged across trials of each type. Fig. S5 illustrates average time-frequency spectrograms and SDF for fast and slow trials, suggesting that there is no systematic transient activity in either the LFP signals or the SDFs that could synthetically couple the spikes to LFPs. We further quantitatively compared the magnitude of transient responses (i.e., sudden changes of activity) in high-gamma power/SDF between fast and slow trials to examine if any systematic difference could have caused a difference in the coupling of spikes to LFP. To this end, we first calculated the high-gamma power for each time instance by averaging the power across frequencies (180-220 Hz), using the time-frequency spectrum of each trial. Second, we calculated the mean and standard deviation of high-gamma power for each trial. Third, we applied a threshold to find those times with a power deviating by more than three standard deviations from a trial's high-gamma power. The power in the selected times was z-scored and their absolute value was averaged across each trial. Fig. S6 shows the resultant values for the fast and slow trials. Sudden changes are stronger for slow trials ($\rho = 0.021$, two-sided rank-sum test). Assuming that transient responses cause spurious spike-LFP coupling, these results indicate that our observation of a higher SPC in fast, compared to slow trials cannot be attributed to potential differences in the magnitude of transient responses between fast/slow trials.

SPC difference is not an artifact of systematic correlation between spiking and high-gamma power. To measure the correlation between "spike time" and "High-gamma power", we selected spikes based on the aforementioned threshold and next equalized the high-gamma powers (180-220 Hz, 180-230 Hz and 190-240 Hz for animals H, T and C respectively,

frequencies with the maximum SPC difference between fast and slow, as also visualized in Fig 1E and Fig. S10). We extracted parts of the LFP signal within ± 60 ms time-windows surrounding the spikes for each trial. Next, short-time Fourier transform was applied on each LFP segment to calculate the time-frequency map of the high-gamma power. For the time-frequency analysis we used 6ms wide time windows with a 5ms overlap and required a minimum power at the lowest frequency of the high-gamma range (i.e., 180 Hz). For each LFP segment, the values of the time-frequency map were normalized to the maximum power and the powers in the high-gamma range were averaged. Next, average high-gamma powers, at an equal distance from the spike event were averaged. We then calculated the correlation (Spearman correlation r) between time lags from spike time and average high-gamma power surrounding the spike event. A positive correlation would indicate an anti-correlation between high-gamma power and spike and vice versa. We found a significant positive correlation in slow trials for animals H ($r = 0.58$, $\rho < 10^{-5}$) and T ($r = 0.75$, $\rho < 10^{-325}$) (in agreement with a previous documentation by Watson et al (1)), but this was not the case for animal C ($r = 0.04$, $\rho > 0.7$). Applying the same approach on the fast trials showed: animal H: $r = 0.2$, $\rho > 0.12$; animal C: $r = 0.77$, $\rho < 10^{-325}$; animal T: $r = -0.59$, $\rho < 10^{-5}$. Given that monkeys H and T had a larger positive correlation in slow compared to fast trials, one may argue that the reduction of SPC level in slow trials might be due to an anti-correlation between spiking and high-gamma power (due to a potentially smaller signal to noise ratio of LFP power at the time of a spike, in slow trials). However, the above-mentioned correlation results for fast and slow trials for the three animals do not confirm this hypothesis. They indicate that while the correlation between spiking and high-gamma power is significantly positive and larger in slow rather than fast trials in animals H and T, this becomes opposite for animal C (where there is a highly significant positive correlation in fast trials, but no significant correlation in slow trials).

SPC difference is not caused by the difference of inter-spike intervals. We controlled the robustness of the SPC effect against potential confounds which are related to the distribution of inter-spike interval (ISI), such as refractoriness and spike bursts. We therefore examined if the difference of SPC between fast and slow trials could be due to differences between the ISI distributions. Hence, we randomly sub-selected the spikes such that the median of the ISI distribution became either 1) higher for fast, rather than slow trials 2) higher for slow, rather than fast trials 3) equal between the two trial types, and then compared the SPC (within 195-200 Hz, the frequency range with the maximum SPC modulation - see Fig. 1A) between the two. For example, to reach spike trains where the median of the ISI distribution is higher for fast, rather than slow trials, we randomly selected an equal number of spikes from each trial and calculated the distribution of ISI for the trial. Then median of ISI was compared to a predefined threshold; if the median was higher than the threshold, we decided to consider the selected spikes and computed the SPC based on them. Otherwise, the spike selection routine was repeated up to a maximum of 1000 times to reach an ISI distribution with a median higher than the threshold. The number of spikes selected randomly for each repetition was equal to the original SPC method (*see Methods*). Similarly, for slow trials we took the same approach to reach spike trains with a median ISI lower than the predefined threshold. To provide a stable value for average SPCs in fast and slow groups, we repeated the algorithm for 100 times. To change fast trials so that they had lower\same ISI medians compared to the slow trials, we used a similar routine as described above, with updated thresholds. Fig. S7 shows the average SPC and the ISI distribution for the three median ISI conditions described above. The figure shows that SPC in fast trials are always significantly larger than for slow trials, regardless of ISI arrangements ($p<0.01$, permutation test).

Analysis of SPC without LFP power equalization. We calculated high-gamma SPC (180-220Hz) before equalization of the high-gamma spectra between fast and slow trials. The SPC was calculated using the same algorithm used for Fig.1; for each of the 5Hz frequency bands between 180-220 Hz, the SPC was calculated for a given trial. Next, SPCs were smoothed using a moving

average with a window width of 4Hz. The average smoothed SPC per trial showed that the high gamma SPC remained significantly higher in the fast compared to the slow trials even before the high-gamma power was equalized ($\rho < 0.012$, two-sided sign-test).

SPC disappears by shuffling spike times. To ensure the SPC difference is caused exclusively by the spike times, rather than the temporal phase pattern of the LFPs, the SPC strength is further compared between the fast and slow trials after the spike times are shuffled. To this end, we used the fast and slow trials which were equal in their high-gamma power and spike rates (similar to Fig. 1E-*see Methods*). First, the spike times were randomly shuffled (uniformly in time) in each trial and then the SPC was calculated for 195-200 Hz (the frequency with maximum modulation-see Fig. 1A). Second, we calculated the average SPC for each trial across 10,000 repetitions. Third, we performed a statistical test by shuffling the SPCs between fast and slow trials and calculated the difference between average SPCs in the pseudo-fast and pseudo-slow resultant. We performed this permutation test for both the shuffled and original SPCs and compared the main difference between the average SPC of the fast and slow trials with the shuffled trials. These control analyses indicate that in contrast to the original data ($P<0.006$, permutation test), the SPC difference disappears after shuffling the spike times ($P > 0.7$, permutation test) (Fig. S8A). Furthermore, we used the fast trials (where spike phase coupling was large enough) to visualize the high-gamma fluctuations in the shuffled and original condition, for the frequency range of 180-220 Hz (see Fig. S8B). These results particularly show how temporally organized spikes of the original data occur relative to the high-gamma phase. The same routine as described for Fig. 1E was performed for this visualization.

Analysis of cross-correlograms. Spike-spike coupling (SSC) was measured by computing the cross-correlograms between simultaneously recorded neuron pairs, using an unbiased correlation method. Due to the small amount of data available (especially because of the number of trials passing our criterion to be classified as fast vs slow) for pairs of neurons with an inter-electrode distance larger than 2, and to avoid interpretation complexities, we focused here on pairs of simultaneously recorded units with inter-electrode distances of 1 & 2. To equalize the spike rate across trials we applied an algorithm similar to the one we used for spike-LFP phase coupling analyses. We calculated SSC for ±10ms time lags, the interval with the largest observed SPC strength in high-gamma (see Fig. S11). We repeated the calculation by randomly selecting spikes (1,000 times) and computed the average cross-correlogram for a given neuron pair in a trial. Then, the strength of SSC was measured in high-gamma frequency (180-220 Hz) using Welch's power spectral density routine. This routine was used in 7ms wide time windows and a 3ms of overlap, selected based on the minimum requirements to capture the power of 180 Hz frequency components. We further found that the SSC strength in the high-gamma frequency range (180-220 Hz) was significantly stronger in fast rather than the slow trials ($\rho < 0.0075$, permutation test with 10,000 shuffles between fast and slow SSCs). Fig. S9 illustrates the average SSC for the fast and slow trials and illustrates that the inter-neuronal synchrony is significantly stronger in the fast trials, in agreement with our high-gamma SPC results.

Spike-triggered average of the high-gamma LFP (STA_{HG}). We used a similar routine as described for Fig. 1E (for monkey H) to sketch the spike-triggered average within high-gamma (STA_{HG}) for the other two animals (monkeys C and T). Because the number of spikes and trials in both of these animals was small, we calculated the average STA_{HG} across 1,000 repetitions per trial. Fig. S10 shows the average STA_{HG} across different trials for monkeys C and T. Importantly, in-line with Fig. 1B, where the modulation of SPC for monkey T is smaller in magnitude compared to the other two animals, here we also observe a less distinction between the peak-to-peak amplitudes of the fast and slow group for monkey T compared to the other two.

High-gamma SPC is not a consequence of applying digital filters. To control for any potential side effect caused by the band-pass filters, we calculated the spike-triggered average of LFP (STA_{LFP}) for trials selected in the STA_{HG} analysis (see *Methods* for Fig. 1E). To this end, we averaged the raw LFP segments in the ±15ms time intervals surrounding each spike and then normalized the STA_{LFP} using a z-score transform. Fig. S11 clearly demonstrates a high-gamma fluctuation around the spike event time (0 ms) for the fast trials, while this is not the case for slow trials.

SPC for the target-out condition. The SPC was calculated for trials where the target stimulus was presented outside the RF (target-out). To calculate the SPC strength, we used the same routine as for the target-in condition (Fig. 1-see *Methods*). The result for monkeys H and T (animals with a large enough number of target-out trials) demonstrate no frequency band with a significant SPC difference between fast and slow trials (Fig. S12; blue vs. red traces) ($\rho < 0.0006$ two-sided sign test, controlled for multiple comparisons, using Bonferroni).

STA_{HG} for different inter-electrode distances. We have expanded on Fig. 3A by plotting the spike-triggered LFP (within high-gamma) for different distances between the spike-providing and LFP-providing electrodes (Fig. S13*B*). To this end, we calculated the spike-triggered high-gamma LFP (STA_{HG}) for fast and slow trials with an equal high-gamma power (180-220 Hz). This shows in-line with Fig. 3A that the coupling of spikes to high-gamma phase (quantified by the peak-to-peak amplitude difference of the STA_{HG}) does not decrease by increasing the inter-electrode distance, confirming that our measured SPC is not an artifact of a spectral leakage from spikes onto LFPs. Moreover, to examine if the dependence of SPC on response time is confounded by leakage, the average STA_{HG} across all electrode distances higher than 0 (1 - 4) is calculated for fast and slow trials, separately (Fig. S13*C*). Results clearly show that the peak-to-peak amplitude of STA_{HG} is larger for fast rather than slow trials even though spikes and LFPs are chosen from separate electrodes, suggesting that the dependence of SPC on behavior is not associated to the spike's leakage onto LFP.

SPC is a more reliable predictor of RT, compared to the spike rate. We compared the discriminability of RT using either spike rate or SPC. To this end, we applied spike thresholding and power equalization (similar to the main analysis) and calculated the SPC for each of the 5Hz sub-bands of high-gamma (180-220Hz) in 10,000 independent repetitions of spike selection per trial. The area under the ROC curve (AUC) was calculated to determine the difference between fast and slow trials, for each repetition using high-gamma SPCs, within each 5Hz sub-band. The AUCs were next averaged across the high-gamma sub-bands. Fig. S14 demonstrates the average and standard deviation of the high-gamma SPC-based AUC across spike shufflings for the three animals. Moreover, we calculated the AUC based on spike rates in the fast and slow trials after applying the spike count thresholding. The results show a significantly larger RT discrimination based on high-gamma SPC compared to that of the spike rate ($\rho < 10^{-3}$, permutation test using 10,000 repetitions) for two of the animals (monkeys C & H), while this discrimination is larger

for spike rate than SPC in animal T ($\rho < 10^{-3}$, permutation test with 10,000 repetitions). These results demonstrate that SPC predicts RT well above the chance level for all animals, while the spike rate discriminates RT well for only one (animal T) and near to the chance level for other animals (H & C). These suggest that SPC, rather than the spike rate is a more reliable predictor of behavioral reaction time.

The SPC effect's difference with the literature could not be attributed to task/cortical area differences. We investigated if the difference between the frequency ranges that show the SPC effect (across V4(2)/MT), could be due to any potential influence of the average spike rate or monitor refresh rate on the SPC. V4 neurons fire at a low rate, varying between 15-20 Hz in different studies (3–5). In our data (from MT), neurons fire at 33, 23, 30 Hz for monkeys H, C and T, respectively. Apart from the small difference observed here between the firing rates of V4 and MT (~ 11 Hz), we could hardly imagine a correlation between an area's characteristic spike rate and the frequency for which SPC discriminates reaction time: assuming such a correlation, we expect it to cause a difference in the SPC difference frequency across our animals. However, given the variation of 10 Hz between the characteristic spike rates of the animals, the SPC difference frequency (200 Hz, 208 Hz, 215 Hz for animals H, C and T) does not show any systematic variation (relative to the spike rates) across animals. Regarding the monitor refresh rate, in Fries et al's study in V4, the refresh rate was 120 Hz (6), while in our study it was between 75-76 Hz. We know that the monitor's frame refresh could induce frequency components imposing a spurious phase locking between spike and LFPs. However 1) Fries et al's study prevented the frame refresh to induce a spurious spike phase coupling, since the LFP was low pass filtered with a cut-off frequency of 100 Hz (lower than the frequency of frame rate (120 Hz)). 2) In our data, the monitor refresh rate is equally reflected in the strength of spike-phase coupling in both fast and slow trials (see frequency ~75 Hz in Fig. 1A-C), however the significant SPC difference between fast and slow groups were found for high-gamma frequencies no lower than 180 Hz, far from frequency of monitor refresh rate (~76) and its periodical (152 Hz).

Modeling of the phase-locked or non phase-locked spikes for V4 and MT. We compared the phase-locking of synthetically generated V4 and MT spikes to the gamma or high-gamma oscillations. To this end, we calculated the spike-triggered average of gamma (STA_G) and high-gamma (STA_{HG}) oscillations as well as the histogram of the average instantaneous phase for V4 and MT, respectively, and separately in the conditions where the spikes were phase-locked or not phase-locked to the LFP phase. The results are shown in Fig. S15. The histograms show how spikes are differentially coupled to the LFP phase of the corresponding frequency range (gamma for V4, and high-gamma for MT) in the phase-locked and non phase-locked conditions (V4: $\rho < 10^{-157}$ and $\rho > 0.5$; MT: $\rho < 10^{-157}$and $\rho > 0.9$; Rayleigh test).

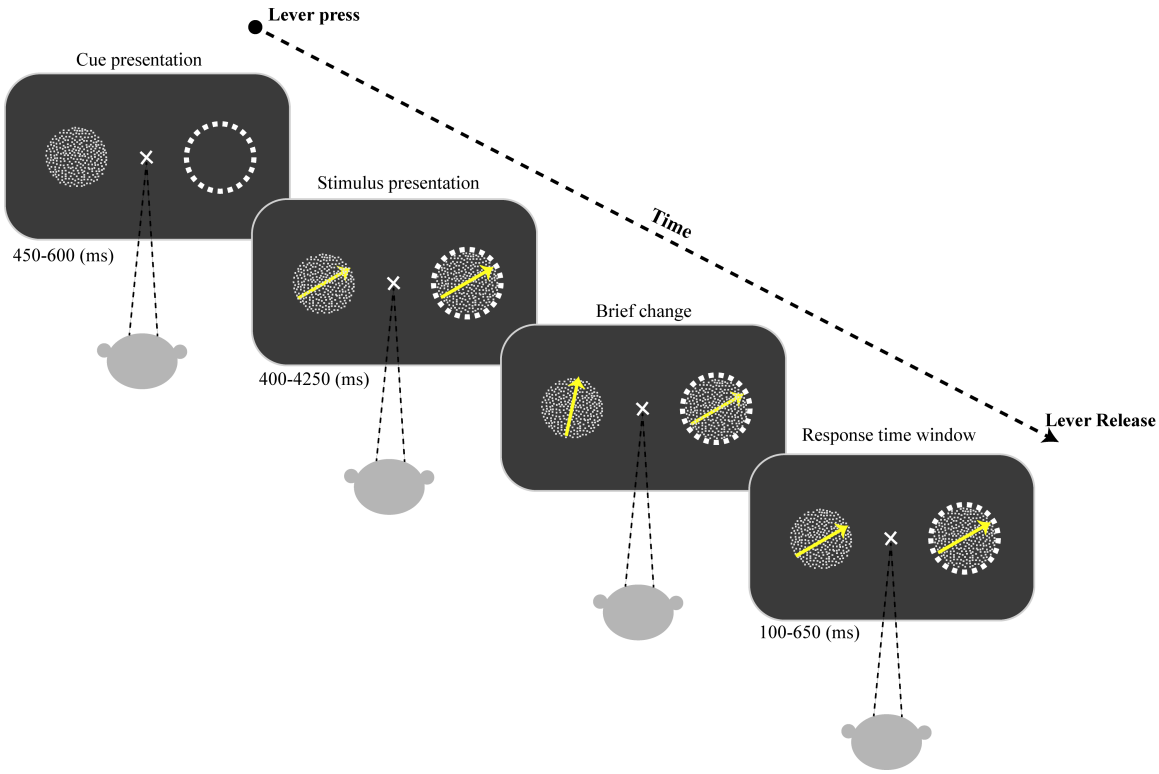

Fig. *S1.* *Behavioral paradigm. The monkey had to touch a lever and maintain its gaze on a central fixation point to start a trial. Next, an eccentric spatial cue briefly appeared on the screen for 450-600ms to indicate the upcoming target stimulus' location. Afterwards, moving random dot patterns (RDPs) were presented inside and outside the receptive field (dashed circle) for a random interval between 400-4250ms. The monkey was rewarded with a juice when releasing the lever within a short response window (100-650ms) in response to a short change in either color, direction or speed (only one type occurred in a trial) of the target RDP. The cross sign indicates the fixation point. The dashed circle was not presented in the experiment.*

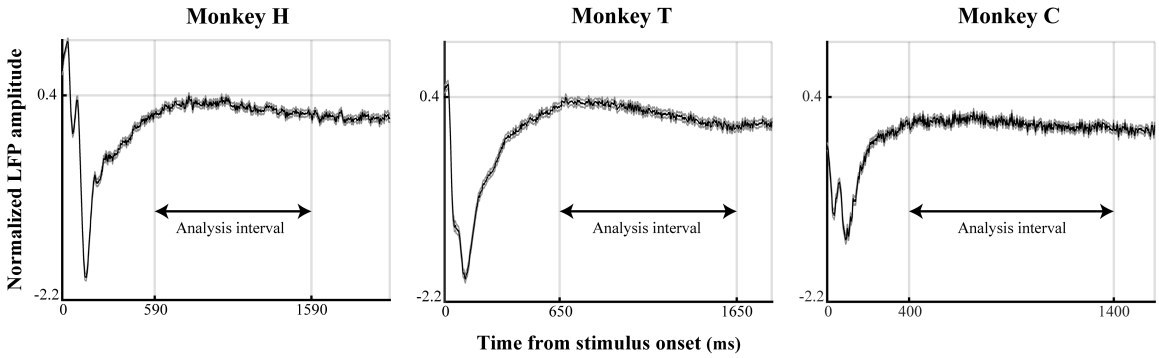

Fig. *S2.* *Time course of averaged LFP aligned to stimulus onset, and the analysis time windows. The black/gray lines demonstrate the average/standard error of mean of LFPs across trials (each trial's LFP was first z-scored). As shown, the analysis intervals are chosen to exclude the stimulus onset-evoked transient responses. The shorter duration of the transient response in animal C could be due to a different visual stimulation; For monkey C, two very small stimuli were presented inside the RF (presumably causing the smaller and shorter transient response), while for the other two animals, only one stimulus (as large as the RF's size) was presented in the RF.*

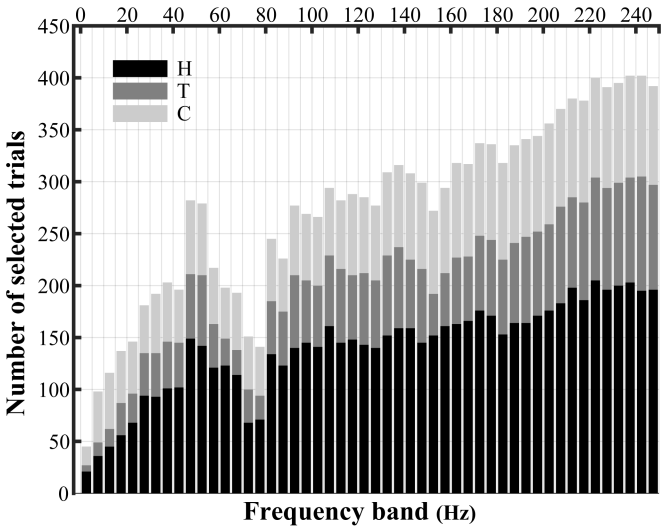

Fig. *S3*. *Stacked bar chart, reflecting the number of selected trials per frequency band. Trials were selected so that the data sets do not show any significant power differences between the fast and slow trials at each frequency band (median significance $\rho > 0.9$, two-sided rank-sum test across 50 frequency bands (1 : 5 : 250 Hz) for the three monkeys)*

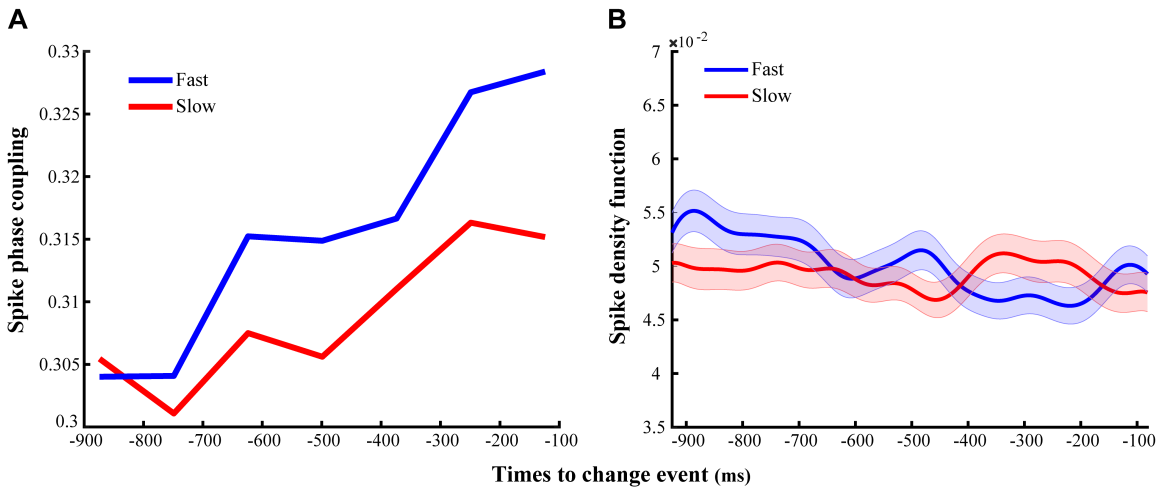

Fig. *S4.* *Temporal evolutions of SPC and SDF for fast and slow groups,* ***A****, time-resolved SPC strength calculated in 250ms sliding windows, overlapped with 125ms. The X-axis shows the SPC strength averaged through each sliding window.* ***B****, average SDF in fast and slow groups is calculated with a Gaussian filtering with 250ms length and σ =50.*

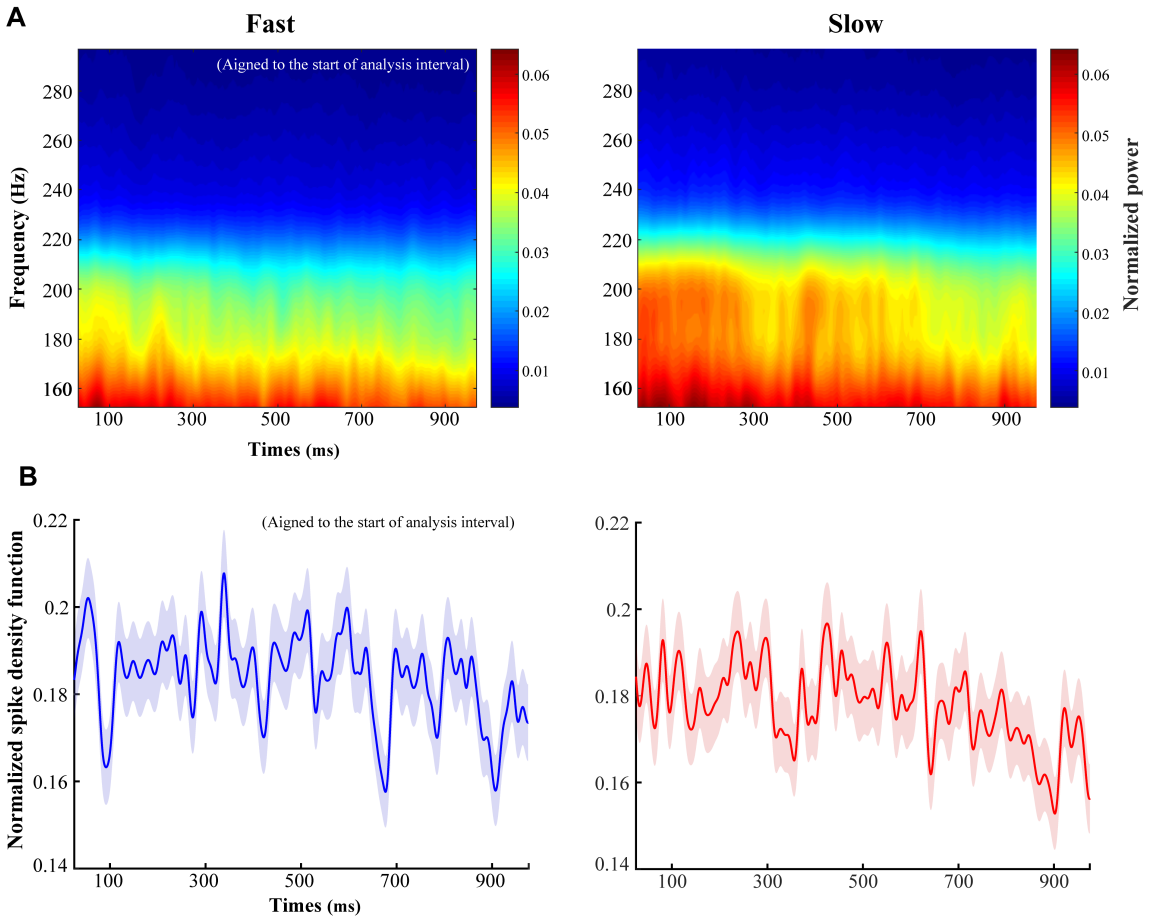

Fig *S5*. *Average time-frequency spectrograms and spike density functions for fast and slow trials (aligned to the start of our analysis interval).* ***A****, average short time Fourier transform of LFPs, with a time resolution of 5ms.* ***B****, average spike density function, with a time resolution of 1ms.*

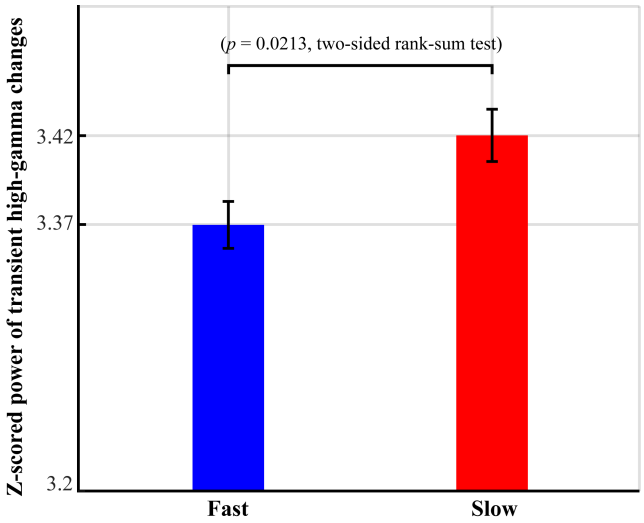

Fig. *S6.* *Power of high-gamma in transient changes. The bars show the average normalized high-gamma power for sudden changes of high-gamma in fast and slow trials.*

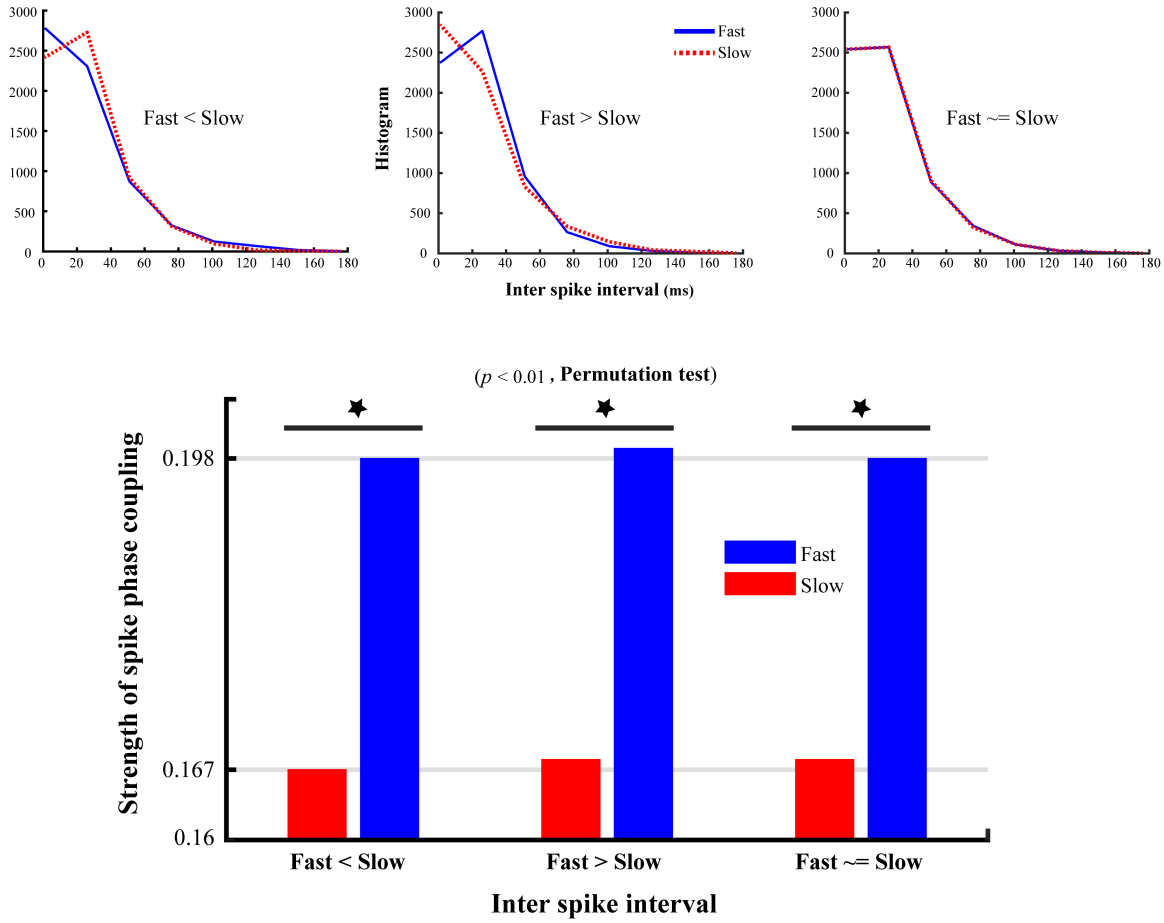

Fig. *S7.* *The effect of spike trains' inter spike interval distribution on SPC in fast and slow groups. The bar plot shows the average high-gamma SPC for when ISIs in fast trials were higher/ lower than or the same as slow trials. The stars indicate conditions with a significant difference between fast and slow SPCs (p<0.01, permutation test). Top curves show the ISI histograms for trials of fast and slow in each of the ISI conditions.*

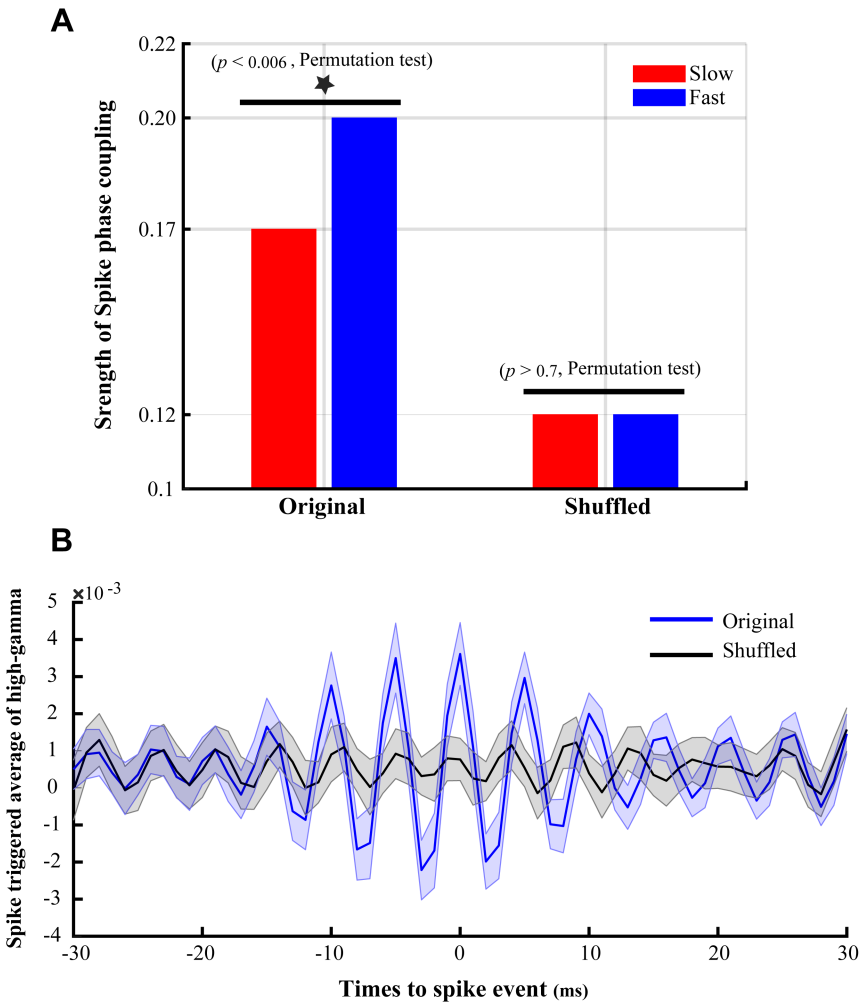

Fig. *S8.* *Comparison of the SPC between the original data and shuffled spikes times,* ***A****, The bar plot shows the average SPC strength (within 195-200 Hz, the frequency with the maximum SPC modulation) for fast and slow trials. The star sign shows the significant difference between fast and slow groups (p<0.006, permutation test).* ***B****, spike-triggered high-gamma (180-220 Hz) LFP based on the original and shuffled spike trains.*

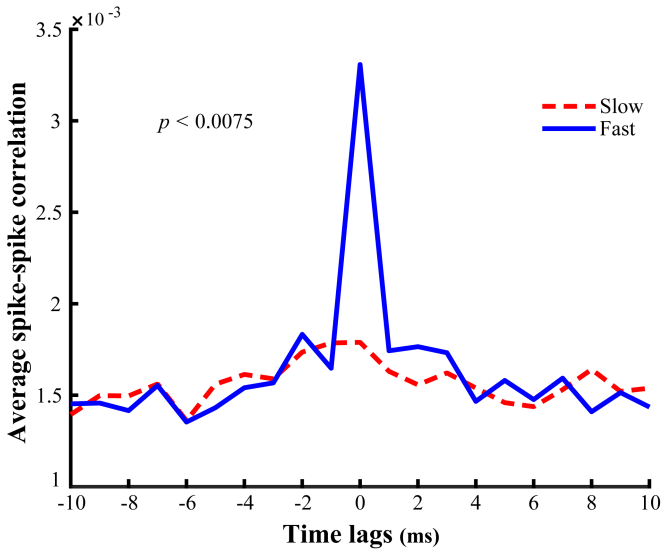

Fig. *S9.* *Analysis of spike-spike correlations (SSC) segregated by RT. The blue and red lines are average cross-correlograms for simultaneously recorded neuron pairs in fast and slow trials, respectively. The SSC strength in the high-gamma frequency range (180-220 Hz) is significantly stronger in fast rather than slow trials (ρ <0.0075, permutation test with 10,000 shuffles between fast and slow SSCs).*

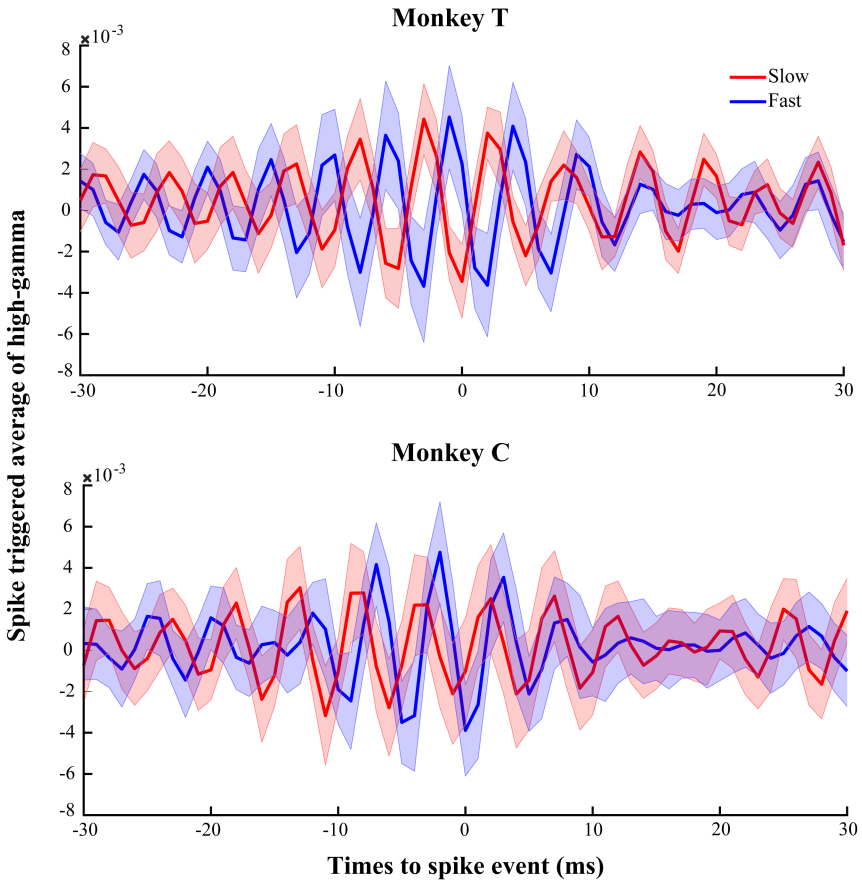

Fig. *S10.* *Spike-triggered average of high-gamma oscillations with the spikes and LFPs from the same electrode. The high-gamma frequency range was between 180-230 Hz and 190-240 Hz for monkeys T and C, respectively.*

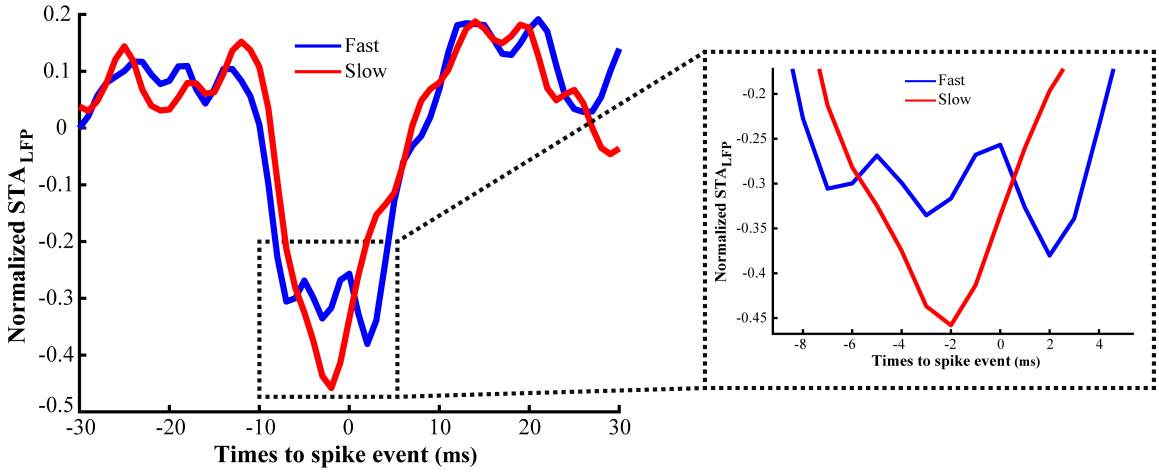

Fig. *S11.* *Spike-triggered average of LFP for fast and slow group of trials.*

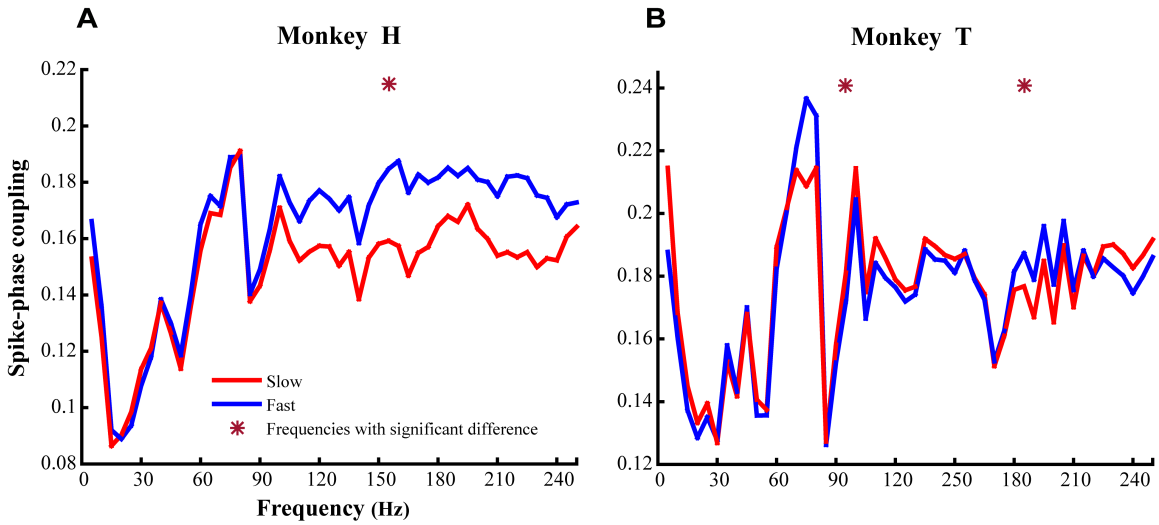

Fig. *S12.* *Spike-phase coupling (SPC) strength for trials where the target stimulus was presented outside the RF. SPC of the fast and slow trials across different frequency bands with a width of 5 Hz distanced by 5 Hz, for the monkeys H and T (animals with a high enough number of trials in the target-out condition). X-axes indicate the upper bound of these frequency bands, and Y-axes represent the SPC values. Stars mark the frequencies with a significant difference between fast and slow trials ($\rho < 0.0006$ two-sided sign test, corrected for multiple comparisons using the Bonferroni method).*

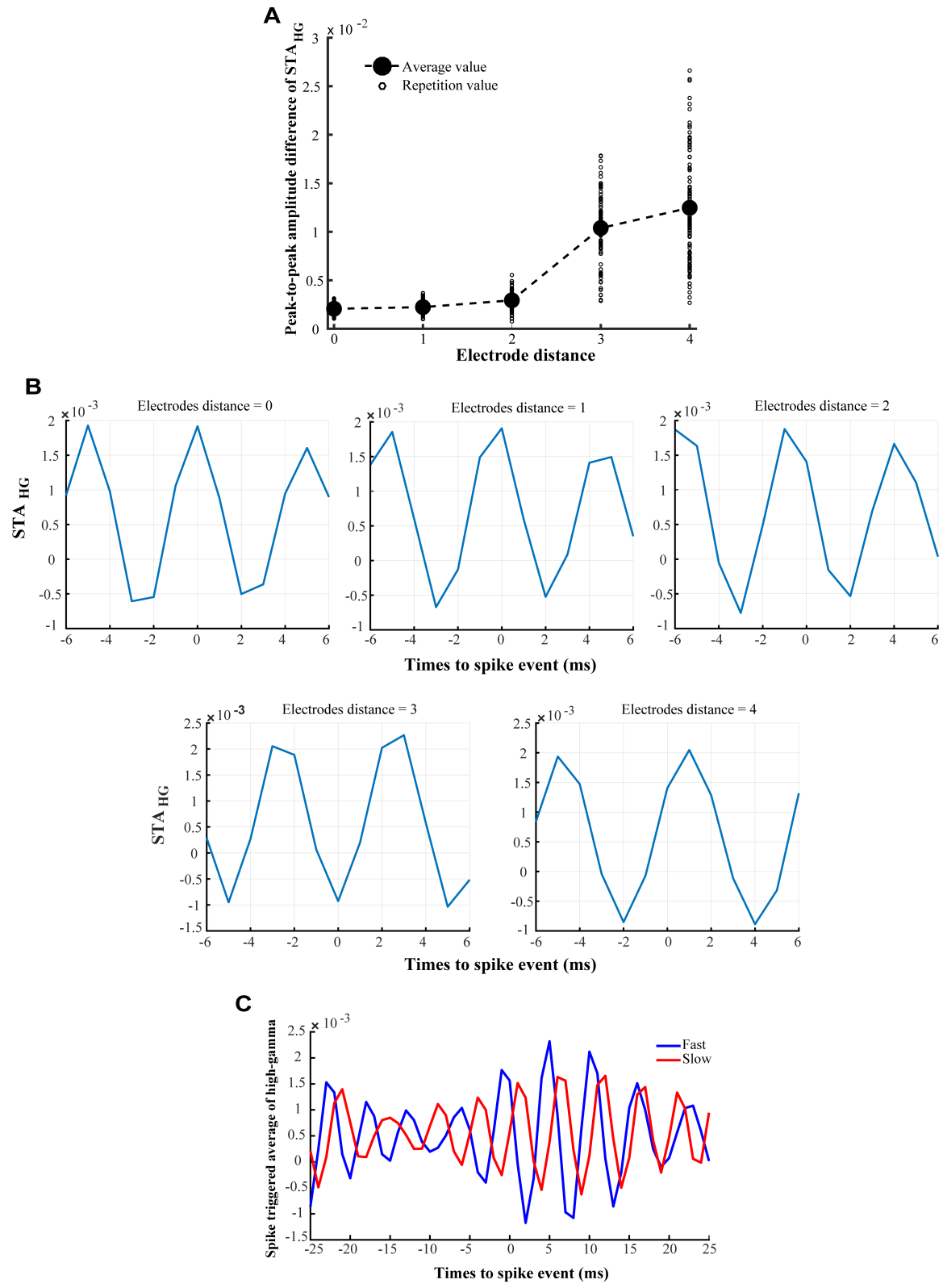

Fig *S13*. *Spike-triggered average of high-gamma LFPs (180-220 Hz) for spikes and LFPs from the same or separate electrodes.* ***A****, The averaged* STA_{HG} *was computed using the spike and LFP coming from the same (distance = 0) or separate electrodes (distances 1 - 4) (same as Fig. 3A).* ***B****, the* STA_{HG} *corresponding to each of the distances shown in panel A.* ***C****, the spike-triggered*

average of high-gamma frequencies (180-220 Hz) for the two types of trials when spike and LFPs were recorded form different electrodes.

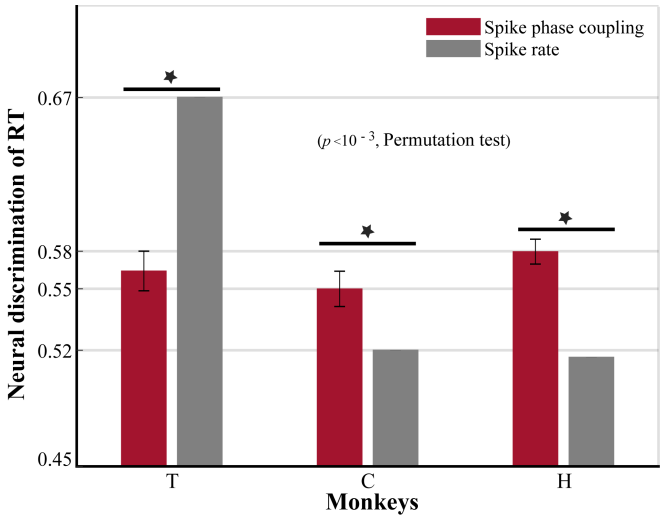

Fig. *S14.* *Neural discrimination of RT, based on high-gamma SPC (180-220 Hz) and spike rates. Stars indicate significant differences between neural discrimination of RT based on high-gamma SPC and spike rate, for each animal ($\rho < 10^{-3}$, permutation test).*

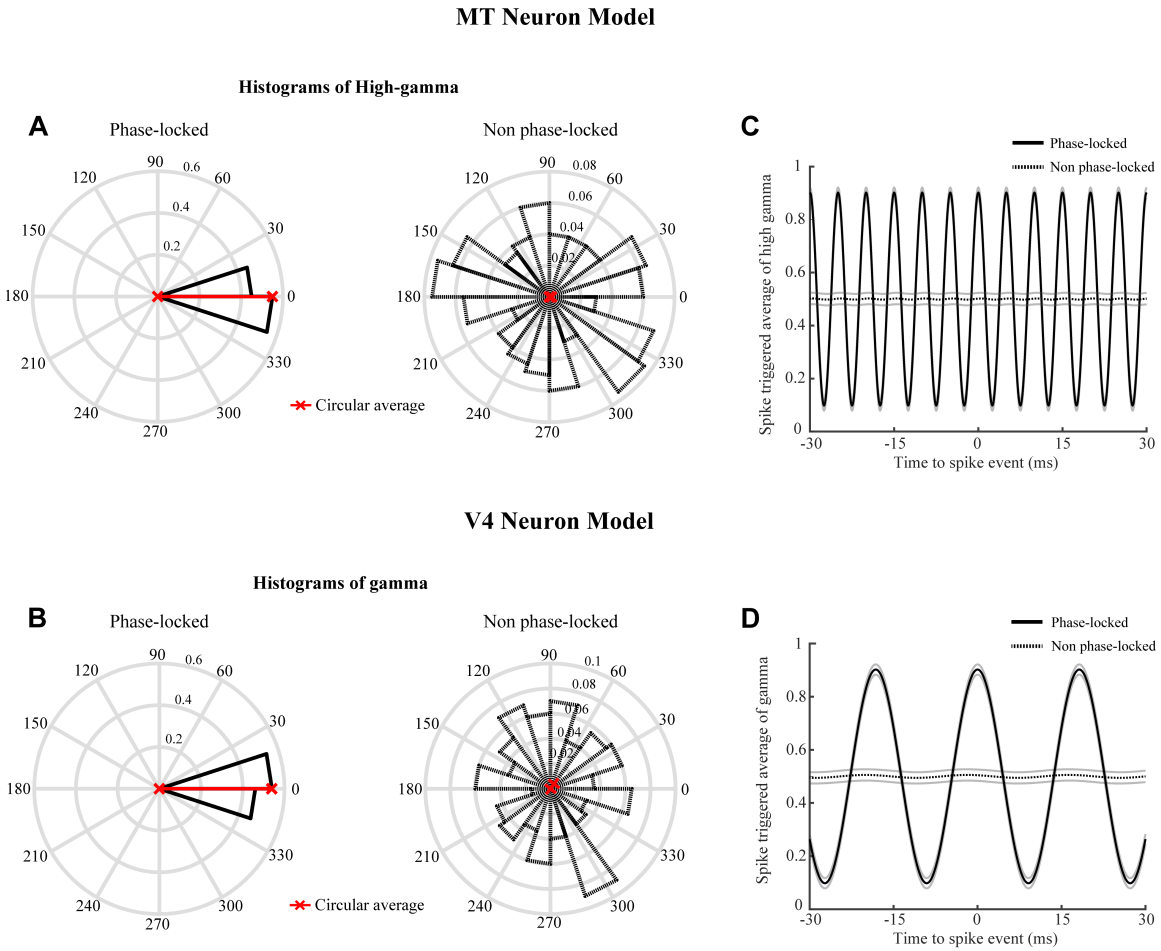

Fig. *S15.* *Characterization of phase-locking for spikes generated by the V4 and MT model neurons, (**A-B**) Histograms of the average instantaneous phase for MT and V4 when spikes are significantly phase-locked to gamma ($p<10^{-157}$, Rayleigh test) and high-gamma ($p<10^{-157}$, Rayleigh test) or distributed randomly ($\rho > 0.5$ for gamma; $\rho > 0.9$ for high-gamma; Rayleigh test) across phase-space for the non phase-locked condition. Each data point represents the average instantaneous phase for each trial (see Results section for details of the modeling data). (**C-D**) spike triggered average of high-gamma (STA_{HG}) and gamma (STA_{G}) oscillations for the phase-locked (solid line) and the non phase-locked (dashed line) condition. The gray line shows the standard error of mean across trials.*

References

1. Watson BO, Ding M, Buzsáki G (2018) Temporal coupling of field potentials and action potentials in the neocortex. *Eur J Neurosci* 48(7):2482–2497.
2. Womelsdorf T, Fries P, Mitra PP, Desimone R (2006) Gamma-band synchronization in visual cortex predicts speed of change detection. *Nature* 439(7077):733–736.
3. Vinck M, Womelsdorf T, Buffalo EA, Desimone R, Fries P (2013) Attentional modulation of cell-class-specific gamma-band synchronization in awake monkey area V4. *Neuron* 80(4):1077–1089.
4. Mitchell JF, Sundberg KA, Reynolds JH (2007) Differential Attention-Dependent Response Modulation across Cell Classes in Macaque Visual Area V4. *Neuron* 55(1):131–141.
5. Desimone R, Schein SJ (1987) Visual properties of neurons in area V4 of the macaque: sensitivity to stimulus form. *J Neurophysiol* 57(3):835–868.
6. Fries P, Reynolds JH, Rorie AE, Desimone R (2001) Modulation of oscillatory neuronal synchronization by selective visual attention. *Science* 291(5508):1560–1563.